HHS Public Access

Author manuscript

J Magn Reson Imaging. Author manuscript; available in PMC 2015 October 01.

Published in final edited form as:

J Magn Reson Imaging. 2015 October ; 42(4): 954–963. doi:10.1002/jmri.24847.

Thoracic Aorta 3D Hemodynamics in Pediatric and Young Adult Patients With Bicuspid Aortic Valve

Bradley D. Allen, MD[1,*], **Pim van Ooij, PhD**[1], **Alex J. Barker, PhD**[1], **Maria Carr, RT**[1], **Maya Gabbour, MD**[2], **Susanne Schnell, PhD**[1], **Kelly B. Jarvis, BS**[1], **James C. Carr, MD**[1], **Michael Markl, PhD**[1,3], **Cynthia Rigsby, MD**[2], and **Joshua D. Robinson, MD**[4,5]

[1]Department of Radiology, Feinberg School of Medicine, Northwestern University, Chicago, Illinois, USA

[2]Department of Medical Imaging, Ann & Robert H Lurie Children's Hospital of Chicago, Chicago, Illinois, USA

[3]Department Biomedical Engineering, McCormick School of Engineering, Northwestern University, Chicago, Illinois, USA

[4]Division of Pediatric Cardiology, Ann & Robert H Lurie Children's Hospital of Chicago, Chicago, Illinois, USA

[5]Department of Pediatrics, Feinberg School of Medicine, Northwestern University, Chicago, Illinois, USA

Abstract

Background—To evaluate the 3D hemodynamics in the thoracic aorta of pediatric and young adult bicuspid aortic valve (BAV) patients.

Methods—4D flow MRI was performed in 30 pediatric and young adult BAV patients (age: 13.9 ± 4.4 (range: [3.4, 20.7]) years old, M:F = 17:13) as part of this Institutional Review Board-approved study. Nomogram-based aortic root Z-scores were calculated to assess aortic dilatation and degree of aortic stenosis (AS) severity was assessed on MRI. Data analysis included calculation of time-averaged systolic 3D wall shear stress (WSS_{sys}) along the entire aorta wall, and regional quantification of maximum and mean WSS_{sys} and peak systolic velocity (vel_{sys}) in the ascending aorta (AAo), arch, and descending aorta (DAo). The 4D flow MRI AAo vel_{sys} was also compared with echocardiography peak velocity measurements.

Results—There was a positive correlation with both mean and max AAo WSS_{sys} and peak AAo vel_{sys} (mean: r = 0.84, $P < 0.001$, max: r = 0.94, $P < 0.001$) and AS (mean: $r_S = 0.43$, $P = 0.02$, max: $r_S = 0.70$, $P < 0.001$). AAo peak velocity was significantly higher when measured with echo compared with 4D flow MRI (2.1 ± 0.98 m/s versus 1.27 ± 0.49 m/s, $P < 0.001$).

Conclusion—In pediatric and young adult patients with BAV, AS and peak ascending aorta velocity are associated with increased AAo WSS, while aortic dilation, age, and body surface area

[*]Address reprint requests to: B.D.A., Department of Radiology, Northwestern University, 737 N. Michigan Avenue, Suite 1600, Chicago, IL 60611. bdallen@fsm.northwestern.edu.

do not significantly impact AAo hemodynamics. Prospective studies are required to establish the role of WSS as a risk-stratification tool in these patients.

Bicuspid aortic valve (BAV) is the most commonly diagnosed congenital heart defect with a prevalence ranging from 0.5 to 2% of the population[1] and is often coincident with other congenital cardiovascular diseases, particularly left-sided obstructive lesions such as coarctation of the aorta.[2] Pediatric BAV patients are known to have larger aortic dimensions than children with trileaflet valves, and are prone to progressive ascending aorta (AAo) dilatation.[3] As these patients progress into adulthood, they are at increased risk for aortic dissection as a result of the disease[4]; however, the risk of primary cardiac events in childhood is minimal.[5] Nonetheless, when diagnosed at an early age, BAV patients may require surgical intervention to normalize valve function and alter thoracic aorta anatomy in hopes of reducing long term risk.[6]

Time-resolved, three dimensional (3D) phase contrast (4D flow) MRI is increasingly used to study the role of cardiovascular hemodynamics in BAV.[7] Recent studies in adult patients have shown that congenitally abnormal valves are associated with altered ascending aortic blood flow including high velocity outflow jet patterns and deranged helix and vortex type flow.[8-12] Moreover, coarctation of the aorta can also result in varied hemodynamics in both the ascending and descending aorta in BAV patients.[13] These hemodynamic alterations can result in changes in aortic wall shear stress (WSS) which have been shown to promote endothelial cell dysfunction and may ultimately lead to vascular remodeling.[14] Elevated AAo WSS resulting from high velocity, asymmetric outflow jets in BAV patients has been hypothesized to play a role in progressive aortic dilatation in this cohort. Recent studies have demonstrated that adults with BAV have systematically higher and more asymmetric WSS relative to age and aortic size matched controls,[9-11,15,16] and recent work by van Ooij et al using 4D flow MRI demonstrated increased volumetric WSS in the ascending aorta of adult BAV patients with aortic valve stenosis.[17] Other hemodynamic parameters such as peak velocity, flow jet angle,[18] and outflow eccentricity (flow displacement)[19] have also been used in an attempt to quantify the impact of valvular heart disease on aortic hemodynamics.

In the pediatric population, 4D flow MRI assessment has generally been described in small studies or case reports that have focused on patients with complex congenital heart or vascular defects or on postsurgical hemodynamics such as Fontan circulation.[20-23] Truong et al recently used 2D phase contrast of the right pulmonary artery to measure WSS in children with pulmonary artery hypertension.[24] However, the impact of BAV on changes in blood flow and the association with age and aortic size is poorly understood. In this pilot study, our aim was to describe the influence of BAV on thoracic aorta hemodynamic parameters in a group of pediatric and young adult patients using 4D flow MRI.

Materials and Methods

Patient Selection and Characteristics

In accordance with an Institutional Review Board (IRB) approved and HIPAA compliant protocol, over the course of 24 months, n = 30 (age: 13.9 ± 4.4; range: 3.4, 20.7) years old, M:F = 17:13) BAV patients were consecutively included and had 4D flow MRI included as

a part of their physician-ordered cardiovascular MRI assessment. The majority of patients had multiple indications for MRI as listed by the ordering physicians and these indications included assessment of: BAV function (n = 26), aortic size and morphology (n = 14), aortic coarctation (n = 10), and right ventricular size and function (n = 1). All patients (or their surrogate decision maker for patients under the age of 18 years old) were provided and signed an IRB-approved notification of informed consent for the addition of the 4D flow sequence. A total of 10 patients were not able to fully cooperate during the MRI examination and were imaged using general anesthesia performed under the guidance of a pediatric anesthesiologist per the institutional clinical protocol. The BAV cohort included n = 25 right/left coronary leaflet fusion (R/L) patients and n = 5 right/noncoronary leaf-let patients (R/N) as defined by Siever's classification.[25] To account for the wide range of patient age and size, aortic root Z-scores and tubular ascending aorta Z-scores were calculated for each patient from MRI aortic measurements and body surface area (BSA) at time of scan using EchoIMS (Merge Healthcare, Chicago, IL). The Z-score is a nomogram-based metric for assessing aortic dilatation in pediatric patients in which a Z-score between −2 and +2 is considered normal.[26,27] While EchoIMS provides ultrasound-derived normative data, there is currently no MRI-specific database, and as such, this method of normalization is the best available alternative and supported by previous studies.[28] Aortic valve stenosis (AS) and Aortic Insufficiency (AI) were visually assessed by a clinician as part of the standard clinical MRI evaluation and described as "none", "trace", "mild", "moderate", or "severe" in the clinical MRI report. Results were collected from the clinical MRI report and then assigned an ordinal value ranging from 0–4 (0 = none, 1 = trace, 2 = mild, 3 = moderate, 4 = severe).

MR Imaging

Cardiac MRI scans were performed at 1.5T (MAGNETOM Avanto or Aera, Siemens, Germany). Free-breathing, ECG- and respiratory navigator gated 4D flow MRI data were acquired with full volumetric coverage of the entire thoracic aorta and three-directional velocity encoding. Data were acquired at each cardiac time frame as a set of anatomically-weighted magnitude data and three separate phase contrast acquisitions (one for each spatial dimension). The result is a fully characterized 3D velocity field within the acquired 3D data volume. The 4D flow scan characteristics for this cohort were: field of view: 300–320 × 180–260 mm^2, matrix size: 128–192 × 72–156, spatial resolution = 2.2–3.5 × 1.7–2.5 × 2.0–4.0 mm^3, temporal resolution = 37.6–40.8 ms, TE/TR/FA = 2.3–2.6 ms/4.7–5.1 ms/15°, and velocity sensitivity (VENC) = 150 – 400 cm/s as suggested by 2D phase contrast VENC settings established in the clinical imaging protocol. In addition to 4D flow MRI, balanced steady state free precession images in standard cardiovascular views as well as 2D phase contrast scans were prescribed as appropriate for CMR assessment of patients with aortic valve disease.

Data Analysis

All 4D flow data were corrected for Maxwell terms, velocity aliasing, and eddy currents using Matlab-based in-house software (Mathworks, MA).[29] A 3D phase-contrast MR angiogram (PC-MRA) was generated from the corrected data and a peak systolic 3D segmentation of the thoracic aorta was performed (Mimics, Materialise, Belgium). Using the

time-resolved velocity field captured with 4D flow MRI and this 3D segmentation, 3D blood flow visualization was performed in the PC-MRA data using dedicated software (Ensight, CEI, Apex, NC) to generate both time-resolved pathlines and peak systolic streamline representations of the 3D flow field (Fig. 1A). Based on the 3D segmentation, time-resolved 3D WSS along the entire vessel wall was calculated using the same approach in the aorta as van Ooij et al[17] and originally developed by Potters et al[30,31] (Fig. 1B) where shear rates are derived from 1D smoothing splines fitted through the tangential wall velocities at each pixel along the wall then multiplied by the dynamic viscosity of blood. To define systole in each patient, the velocities within the total segmented aorta were averaged for each cardiac time frame and peak systole was defined as the cardiac time frame with highest velocity. Time-averaged systolic values for absolute WSS (WSS_{sys}) were defined as the average over the five cardiac time frames centered on the peak systolic time frame (peak systolic phase ± 2 phases). The peak systolic velocity (vel_{sys}) was defined as the spatiotemporal maximum within the aorta region of interest (AAo, arch, DAo) over the five systolic time frames centered on peak systole. WSS_{sys} maximum intensity projections (MIP) were mapped onto a sagittal view of each aorta for qualitative review and regional analysis. The aorta was further divided into AAo, arch, and descending aorta (DAo) regions (Fig. 1B). Regional dividing lines were drawn orthogonal to the visually assessed vessel centerline with the AAo starting at the sinus of valsalve, the AAo/arch division occurring just proximal to the brachiocephalic trunk, the arch/DAo division mirroring this level just proximal to where the left pulmonary artery crosses the descending aorta, and the DAo ended at the level of the diaphragm. All branches of the aortic arch were excluded from the segmentation. Maximum and mean WSS_{sys} as well as vel_{sys} were calculated in each region. The maximum WSS_{sys} was defined as the average of the top 5% of all values in a region to account for noise within the data.

Subgroup Assessment

In this study cohort, 10 patients had coincident BAV and aortic coarctation. Of the patients with coarctation, 70% (n = 7) had previous coarctation repair. To explore how coarctation or coarctation repair alters thoracic aorta hemodynamics in pediatric BAV patients, a subgroup analysis was performed to compare WSS_{sys} and vel_{sys} at the three aortic regions between patients with and without a history of coarctation or coarctation repair. Also, previous studies have identified AAo hemodynamic variation based on valve morphology,[9] so an additional subgroup comparison between patients with R/L and R/N BAV fusion patterns was performed.

Echocardiography Comparison

Echocardiography is regularly used for quantitative hemodynamic assessment of aortic valve pathology. Aortic valve peak velocity was available from a recent echocardiography study in 28 patients (93%), and these data were used to correlate echo measured velocity with 4D flow peak velocity. The time difference between echo assessments on MRI in these patients was 0.3 ± 0.5 years.

Aortic Growth Rates

Given the interest in understanding the impact of aortic hemodynamics on AAo dilatation in this cohort, MR measurements of aortic dimensions were collected from previous studies to calculate ascending aorta growth rate. This data was available 13 patients (43%). Growth rate was defined as the change in aorta diameter divided by the time between scans in years, and both the indexed aortic growth rate (indexed to BSA and measured in mm/m^2/year) and absolute aortic growth rate (mm/year) were calculated for the aortic root and the AAo.

Statistical Analysis

To identify relationships between hemodynamic parameters and age, BSA, Z-score, stenosis grade, echo-measured peak velocity, and aortic growth rates, linear regression was performed and Spearman (r_S, for ordinal AS/AI data) or Pearson (r, for all continuous data) correlation coefficients were calculated. To further isolate significant drivers of hemodynamic variability, linear modeling using AS, AI, root Z-score, BSA, and age was performed for AAo max and mean WSS_{sys} and peak velocity. Univariate analysis of variance (ANOVA) with a post hoc Bonferroni *P*-value adjustment for between-group comparison was used in the coarctation subgroup analysis. A *P*-value < 0.05 was considered significant for all statistical tests. Nonpaired t-tests were used to compare R/L and R/N fusion patterns. Bland-Altman analysis was performed and a paired t-test was used to compare echocardiographic and 4D flow AAo peak velocity measurement.

Results

Patient Characteristics

Using a Z-score > 2 to define dilation, n = 17 subjects (57%) had aortic root dilatation (cohort average = 2.5 ± 1.7) and n = 14 patients (45%) had ascending aorta dilation (cohort average = 2.3 ± 2.3) (Table 1). The average body surface area was 1.47 ± 0.41 m^2. AS was diagnosed in n = 13 patients (43%) and the cohort average severity was 1.0 ± 1.3, with n = 1 patients being classified as severe, n = 4 as moderate, n = 7 as mild, and n = 1 as trace. AI was diagnosed in n = 12 patients (40%) and the cohort average severity was 0.6 ± 0.9, with no patients being classified as severe, n = 1 as moderate, n = 5 as mild, and n = 6 as trace.

Data Acquisition, Processing, and Visualization

4D flow MRI, 3D segmentation and 3D blood flow visualization was performed in all n = 30 patients. Figure 2 demonstrates the resulting 3D segmentation (Fig. 2A), WSS_{sys} MIPs (Fig. 2B), and peak systolic streamlines (Fig. 2C) in a patient with normal aortic root dimensions (root Z-score-< 2), mild aortic root dilation (2< root Z-score < 5), and severe dilation (root Z-score > 5).

Regional Wall Shear Stress and Velocity

Regional hemodynamic findings are listed in Table 2. There was a positive correlation between mean and max AAo WSS_{sys} and peak AAo vel_{sys} (mean AAo WSS_{sys}: r = 0.84, *P* < 0.001; max AAo WSS_{sys}: r = 0.94, *P* < 0.001) as well as AS (mean AAo WSS_{sys}: r_S = 0.43, *P* = 0.02; max AAo WSS_{sys}: r_S = 0.70, *P* < 0.001) demonstrating a strong, direct

relationship between the presence of high velocity outflow and increased AAo WSS_{sys} (Fig. 3). Neither mean nor max AAo WSS_{sys} correlated with age or BSA. Peak AAo vel_{sys} had a significant positive correlation with age (r = 0.42, P = 0.02), BSA (r = 0.48, P = 0.01), and AI (r_S = 0.52, P = 0.004). There was no correlation between mean or max WSS_{sys} in the AAo and aortic root Z-score (mean: r = −0.24, P = 0.21, max: r = −0.13, P = 0.50). Linear modeling of WSS and velocity in the AAo using AS, AI, root Z-score, BSA, and age as model parameters identified AS as the only parameter significantly correlated with mean AAo WSS_{sys} (β: 0.08, P = 0.02), max AAo WSS_{sys} (β: 0.28, P < 0.001), and peak AAo velocity (β: 0.23, P < 0.001)

Additionally, WSS in the arch and DAo was impacted by presence of aortic coactation or coarctation repair which negatively correlated with mean DAo WSS_{sys} (r_S = −0.38, P = 0.04) but positively associated with max DAo WSS_{sys} (r_S = 0.50, P = 0.01) and max arch WSS_{sys} (r_S = 0.53, P = 0.003), thus motivating subgroup analysis in these cohorts.

Subgroup Analysis: Aortic Coarctation and Coarctation Repair

Patients who had unrepaired aortic coarctation (n = 3, 7.8 ± 5.2 years old) tended to be younger than patients without coarctation (n = 20, 13.7 ± 3.6 years old, P = 0.06) or those with coarctation repair (n = 7, 16.9 ± 4.2 years old, P = 0.006). Otherwise, the groups were similar, without significant differences in aortic root Z-score (P = 0.77), AAo Z-score (P = 0.10), BSA (P = 0.09), or AS (P = 0.78), or AI (P = 0.61) across the three groups (Table 3).

There was no difference between the three groups in AAo mean WSS_{sys} (P = 0.32) or max WSS_{sys} (P = 0.29). However, as shown in Figure 4, relative to patients without coarctation, there was increased max WSS_{sys} in the aortic arch (1.6 ± 0.4 N/m^2 versus 1.1 ± 0.2 N/m^2, P = 0.001) and DAo (1.4 ± 0.3 N/m^2 versus 1.1 ± 0.2 N/m^2, P = 0.009) in patients after coarctation repair. Also, the coarctation repair group had higher max vel_{sys} in the aortic arch (1.4 ± 0.3 m/s) than either the no coarctation group (1.0 ± 0.2 m/s, P = 0.003) or the coarctation group (0.8 ± 0.1 m/s, P = 0.001), as well as higher max vel_{sys} in the DAo than the coarctation group (1.2 ± 0.3 m/s versus 0.7 ± 0.2 m/s, P = 0.02). There was a reduced mean WSS_{sys} in the DAo of patients with aortic coarctation (0.5 ± 0.1 N/m^2) relative to both repaired patients (0.8 ± 0.1 N/m^2, P = 0.02) and patients without coarctation (0.8 ± 0.3 N/m^2, P < 0.001) (Table 3).

Subgroup Analysis: BAV Morphology

The cohort included n = 25 R/L fusion patients and n = 5 R/N fusion patients, and as such is not powered to detect small differences in morphology or hemodynamics between the two groups. There were no significant differences between R/L patients and R/N patients in aortic root Z-score (2.50 ± 1.75 versus 2.68 ± 1.49, P = 0.83), max AAo WSS_{sys} (1.32 ± 0.45 N/m^2 versus 1.35 ± 0.36 N/m^2, P = 0.91), mean AAo WSS_{sys} (0.71 ± 0.19 N/m^2 versus 0.69 ± 0.09 N/m^2, P = 0.77), and peak AAo vel_{sys} (1.26 ± 0.40 N/m^2 versus 1.40 ± 0.42 N/m^2, P = 0.48). There was increased peak DAo vel_{sys} in the R/N group compared with the R/L group (1.19 ± 0.21 m/s versus 0.96 ± 0.20 m/s, P = 0.03).

Echo Versus 4D flow MRI Aortic Valve Peak Velocity

The cohort average echo measured peak velocity was significantly higher than 4D flow measured peak velocity (2.1 ± 0.98 m/s versus 1.27 ± 0.49 m/s, $P < 0.001$), and Bland-Altman analysis demonstrated a systematic underestimation of peak AAo velocity (mean difference: 0.83 ± 0.67 m/s, upper limit: 2.13 m/s, lower limit: −0.48 m/s). (Fig. 5) There is a strong positive correlation between the two measurements of velocity (r = 0.85, $P < 0.001$).

Aortic Growth Rates and Hemodynamics

For the n = 13 patients with a previous MRI scan with ascending aorta dimensions, the average time between scans was 1.9 ± 1.6 years. The indexed aortic root diameter growth rate was −0.9 ± 2.5 mm/m^2/year and the absolute aortic root diameter growth rate was 0.1 ± 1.4 mm/year. The indexed AAo diameter growth rate was −1.2 ± 1.73 mm/m^2/year and the absolute aortic root diameter growth rate was 0.1 ± 1.2 mm/year. There were no significant correlations between aortic root growth rates and max AAo WSS_{sys} (indexed: r = 0.13, $P = 0.68$, absolute: 0.07, $P = 0.84$), mean AAo WSS_{sys} (indexed: r = −0.10, $P = 0.75$, absolute: −0.16, $P = 0.63$), or peak AAo vel_{sys} (indexed: r = 0.06, $P = 0.84$, absolute: r = 0.06, $P = 0.85$). Similar results were found in AAo diameter growth rate with no significant correlations observed in max AAo WSS_{sys} (indexed: r = 0.22, $P = 0.49$, absolute: 0.10, $P = 0.76$), mean AAo WSS_{sys} (indexed: r = 0.51, $P = 0.88$, absolute: 0.50, $P = 0.88$), or peak AAo vel_{sys} (indexed: r = 0.19, $P = 0.56$, absolute: r = 0.15, $P = 0.64$).

Discussion

The current study reveals that in a cohort of pediatric and young adult patients undergoing MRI-assessment of BAV, mean systolic WSS and max systolic WSS both positively correlate with peak systolic velocity and aortic stenosis. After controlling for aortic root Z-score, BSA, and age only aortic stenosis severity appears to drive increases in WSS and velocity in the AAo in these patients. More broadly, our results demonstrate the feasibility of advanced hemodynamic quantification in pediatric BAV patients as young as 3 years old using 4D flow MRI allowing for relative comparisons of these parameters between individuals.

Our findings indicate that, after controlling for severity of vavlular disease in BAV patients, WSS does not correlate with AAo dilation in pediatric patients. This result is somewhat surprising given that results in adult patients suggest an inverse relationship between aorta diameter and reduced AAo WSS[10,32] and that elevated WSS is a hypothesized mechanism for vascular remodeling and progressive aortic dilation as a means to reduce WSS.[14,33,34] Moreover, when looking in isolation at individuals with normal, mild, and severe dilation, the visual WSS trend seems to further suggest this inverse relationship, but at the cohort level the data does not indicate a relationship exists. While we had a large range of diameters, the prevalence of severe valvular disease within our cohort relative to adults in these other studies may have masked this effect, or we may simply be underpowered to detect a significant correlation. It is also possible that the anticipated reduction in WSS with enlarging aorta diameters happens over a long period of time and does not manifest in

younger pediatric patients. Of note, our limited analysis of aortic growth rates in this cohort does not suggest a correlation between hemodynamics and ascending aorta growth rates. However, the number of patients with repeat studies in our cohort is relatively small, and as our data suggests and a recent study by Spaziani et al[35] reports, aortic dilation in children is a very slow process and would require longer follow-up in a larger cohort of patients to adequately assess the impact of altered hemodynamics on aortic growth rates.

Coarctation of the aorta is a common comorbidity in patients with BAV[2] and has been associated with valve morphology.[36] In our study, we were interested in the hemodynamic impact of coarctation on aortic hemodynamics. In adults, 4D flow MRI has been used to study this question and there are reports of increased WSS and flow derangement throughout the aorta independent of valve morphology.[13] We found no significant differences in WSS or velocity in the ascending aorta of patients with coarctation or coarctation repair. Not surprisingly, however, it seems coarctation repair does increase WSS and velocities in the aortic arch and descending aorta relative to BAV patients without aortic coarctation. This finding is potentially important because this hemodynamic alteration could result in subsequent aortopathy at sights of elevated WSS.[37,38] While we noted reduced mean WSS_{sys} in patients with unrepaired coarctation, the conclusions we can draw are limited by the small number of patients (n = 3) that made up this group. Moreover, this cohort tended to be younger and have reduced BSA. These patients likely had smaller diameter descending aortas which can impact accurate assessment of WSS and velocity secondary to the limited voxel coverage of small vessels those results in increased partial volume effects and compromised measurement accuracy. This limitation is particularly important to consider given the surprisingly low velocities in the DAo of nonrepaired coarctation patients.

A challenge in pediatric assessment of aortic hemodynamics is appropriate normalization of measured quantities. Because our cohort spans a large age range (3 to 21 years old) and each patient has a congenital heart defect that has required MRI assessment, establishing criteria for normal WSS was not possible in this study. Moreover, 4D flow MRI assessment in healthy pediatric volunteers also presents an ethical challenge. While aortic dimensions have been extensively reviewed by echocardiography, there is no definitive normative Z-score data for MRI. However, several studies have demonstrated strong agreement of measured aorta dimensions when comparing echocardiography with MRI in pediatric patients,[39,40] and thus the use of echo-derived normative data seems reasonable in the current context. In general, aortic dimensions in pediatric BAV patients correlate well with age,[3] however, in our study WSS did not correlate with age suggesting a possible hemodynamic structure-function relationship within the aorta rather than age-related hemodynamic changes. An additional challenge in this cohort is the use of general anesthesia required in some pediatric patients undergoing MRI. While anesthetic agents may reduce cardiac index and blood pressure in children,[41] the impact of this change outflow hemodynamics is not known.

Our results suggest that 4D flow velocity quantification in the ascending aorta underestimates outflow velocity relative to echocardiographic assessment of peak velocity. This finding is not surprising and has been reported in previous quantification comparisons between these modalities.[42] It is hypothesized that spatial and temporal resolution of 4D flow relative to echo, as well as temporal averaging inherent in the segmented 4D flow

acquisition leads to this result. However, the strong positive correlation between to the two modalities suggests that relative differences in absolute velocities do not invalidate hemodynamic observations made using 4D flow MRI.

The current study is subject to several limitations. First, because these patients were chosen from a BAV population already being sent for MRI, it is possible they have more severe disease relative to a general pediatric BAV population and, thus, our results may be subject to selection bias. Also, because of the size of patient vessels and the spatial resolution of the 4D flow MRI scan, it can be challenging to identify the wall/lumen border during segmentation and our velocity data at the wall and calculated WSS may be more impacted by partial volume effects[43] than a similar study in adults with larger anatomy. Moreover, the use of time-averaged segmentations to study WSS is not ideal in areas where there is significant wall motion during the cardiac cycle such as the aortic root and could result in missing parts of the aortic wall during analysis. Ideally a time-varying segmentation would be used, but this approach dramatically increases processing time and is less-clinically feasible at this time. Future studies on volumetric WSS in the AAo must compare the differences in these two approaches to determine the variability introduced secondary to time-averaged segmentation. Additionally, there is good evidence in the adult BAV literature describing that max WSS location varies based on BAV morphology and can also correspond with aneurysm location.[11,15,44] Our study did not explore the regional variation of WSS within the AAo which may have been impacted by aortic diameter or valve morphology. Finally, a lack of normal controls or a gold standard measure of WSS in this cohort makes it difficult to quantify the absolute hemodynamic changes resulting from BAV.

In conclusion, in pediatric and young adult patients with BAV, aortic stenosis severity and peak ascending aorta velocity are associated with increased ascending aorta WSS. Aortic dilation, age, and body surface area do not significantly impact hemodynamics in these patients. Longitudinal studies correlating changes in WSS and aortopathy over time are needed to establish the role of 4D flow MRI-assessed advanced hemodynamic biomarkers as risk stratification and treatment planning tools in children with BAV.

Acknowledgments

Contract grant sponsor: NIH NHLBI; Contract grant number: R01HL115828; Contract grant sponsor: American Heart Association Scientist Development Grant; Contract grant number: 13SDG14360004.

References

1. Siu SC, Silversides CK. Bicuspid aortic valve disease. J Am Coll Cardiol. 2010; 55:2789–2800. [PubMed: 20579534]
2. Oliver JM, Alonso-Gonzalez R, Gonzalez AE, et al. Risk of aortic root or ascending aorta complications in patients with bicuspid aortic valve with and without coarctation of the aorta. Am J Cardiol. 2009; 104:1001–1006. [PubMed: 19766771]
3. Holmes KW, Lehmann CU, Dalal D, et al. Progressive dilation of the ascending aorta in children with isolated bicuspid aortic valve. Am J Cardiol. 2007; 99:978–983. [PubMed: 17398196]
4. Tzemos N, Therrien J, Yip J, et al. Outcomes in adults with bicuspid aortic valves. JAMA. 2008; 300:1317–1325. [PubMed: 18799444]

5. Mahle WT, Sutherland JL, Frias PA. Outcome of isolated bicuspid aortic valve in childhood. J Pediatr. 2010; 157:445–449. [PubMed: 20400103]
6. Fernandes SM, Khairy P, Sanders SP, Colan SD. Bicuspid aortic valve morphology and interventions in the young. J Am Coll Cardiol. 2007; 49:2211–2214. [PubMed: 17543642]
7. Markl M, Frydrychowicz A, Kozerke S, Hope M, Wieben O. 4D flow MRI. J Magn Reson Imaging. 2012; 36:1015–1036. [PubMed: 23090914]
8. Entezari P, Schnell S, Mahadevia R, et al. From unicuspid to quadricuspid: influence of aortic valve morphology on aortic three-dimensional hemodynamics. J Magn Reson Imaging. 2013; 21:24498.
9. Mahadevia R, Barker AJ, Schnell S, et al. Bicuspid aortic cusp fusion morphology alters aortic three-dimensional outflow patterns, wall shear stress, and expression of aortopathy. Circulation. 2014; 129:673–682. [PubMed: 24345403]
10. Bissell MM, Hess AT, Biasiolli L, et al. Aortic dilation in bicuspid aortic valve disease: flow pattern is a major contributor and differs with valve fusion type. Circ Cardiovasc Imaging. 2013; 6:499–507. [PubMed: 23771987]
11. Hope MD, Hope TA, Crook SE, et al. 4D flow CMR in assessment of valve-related ascending aortic disease. JACC Cardiovasc Imaging. 2011; 4:781–787. [PubMed: 21757170]
12. Hope MD, Hope TA, Meadows AK, et al. Bicuspid aortic valve: four-dimensional MR evaluation of ascending aortic systolic flow patterns. Radiology. 2010; 255:53–61. [PubMed: 20308444]
13. Frydrychowicz A, Markl M, Hirtler D, et al. Aortic hemodynamics in patients with and without repair of aortic coarctation: in vivo analysis by 4D flow-sensitive magnetic resonance imaging. Invest Radiol. 2011; 46:317–325. [PubMed: 21285892]
14. Ben Driss A, Devaux C, Henrion D, et al. Hemodynamic stresses induce endothelial dysfunction and remodeling of pulmonary artery in experimental compensated heart failure. Circulation. 2000; 101:2764–2770. [PubMed: 10851216]
15. Barker AJ, Markl M, Burk J, et al. Bicuspid aortic valve is associated with altered wall shear stress in the ascending aorta. Circ Cardiovasc Imaging. 2012; 5:457–466. [PubMed: 22730420]
16. Meierhofer C, Schneider EP, Lyko C, et al. Wall shear stress and flow patterns in the ascending aorta in patients with bicuspid aortic valves differ significantly from tricuspid aortic valves: a prospective study. Eur Heart J Cardiovasc Imaging. 2013; 14:797–804. [PubMed: 23230276]
17. van Ooij P, Potters WV, Nederveen AJ, et al. A methodology to detect abnormal relative wall shear stress on the full surface of the thoracic aorta using four-dimensional flow MRI. Magn Reson Med. 2014 doi: 10.1002/mrm.25224.
18. den Reijer PM, Sallee D III, van der Velden P, et al. Hemodynamic predictors of aortic dilatation in bicuspid aortic valve by velocity-encoded cardiovascular magnetic resonance. J Cardiovasc Magn Reson. 2010; 12:4. [PubMed: 20070904]
19. Sigovan M, Hope MD, Dyverfeldt P, Saloner D. Comparison of four-dimensional flow parameters for quantification of flow eccentricity in the ascending aorta. J Magn Reson Imaging. 2011; 34:1226–1230. [PubMed: 21928387]
20. Hsiao A, Lustig M, Alley MT, et al. Rapid pediatric cardiac assessment of flow and ventricular volume with compressed sensing parallel imaging volumetric cine phase-contrast MRI. AJR Am J Roentgenol. 2012; 198:W250–W259. [PubMed: 22358022]
21. Markl M, Geiger J, Jung B, Hirtler D, Arnold R. Noninvasive evaluation of 3D hemodynamics in a complex case of single ventricle physiology. J Magn Reson Imaging. 2012; 35:933–937. [PubMed: 22271353]
22. Valverde I, Nordmeyer S, Uribe S, et al. Systemic-to-pulmonary collateral flow in patients with palliated univentricular heart physiology: measurement using cardiovascular magnetic resonance 4D velocity acquisition. J Cardiovasc Magn Reson. 2012; 14:14–25. [PubMed: 22300290]
23. Bachler P, Valverde I, Pinochet N, et al. Caval blood flow distribution in patients with Fontan circulation: quantification by using particle traces from 4D flow MR imaging. Radiology. 2013; 267:67–75. [PubMed: 23297331]
24. Truong U, Fonseca B, Dunning J, et al. Wall shear stress measured by phase contrast cardiovascular magnetic resonance in children and adolescents with pulmonary arterial hypertension. J Cardiovasc Magn Reson. 2013; 15:81. [PubMed: 24034144]

25. Sievers HH, Schmidtke C. A classification system for the bicuspid aortic valve from 304 surgical specimens. J Thorac Cardiovasc Surg. 2007; 133:1226–1233. [PubMed: 17467434]
26. Roman MJ, Devereux RB, Kramer-Fox R, O'Loughlin J. Two-dimensional echocardiographic aortic root dimensions in normal children and adults. Am J Cardiol. 1989; 64:507–512. [PubMed: 2773795]
27. Gautier M, Detaint D, Fermanian C, et al. Nomograms for aortic root diameters in children using two-dimensional echocardiography. Am J Cardiol. 2010; 105:888–894. [PubMed: 20211339]
28. Johnson RK, Premraj S, Patel SS, et al. Quantitative assessment of the entire thoracic aorta from magnetic resonance images. Cardiol Young. 2011; 21:170–177. [PubMed: 21205418]
29. Bock, J.; Kreher, B.; Hennig, J.; Markl, M. Optimized pre-processing of time-resolved 2D and 3D phase contrast MRI data. Proceedings of the 15th Annual Meeting of ISMRM; Berlin, Germany. 2007; abstract 3138
30. Potters WV, van Ooij P, Marquering H, Vanbavel E, Nederveen AJ. Volumetric arterial wall shear stress calculation based on cine phase contrast MRI. J Magn Reson Imaging. 2014:1–12.
31. van Ooij P, Potters WV, Guedon A, et al. Wall shear stress estimated with phase contrast MRI in an in vitro and in vivo intracranial aneurysm. J Magn Reson Imaging. 2013; 38:876–884. [PubMed: 23417769]
32. Burk J, Blanke P, Stankovic Z, et al. Evaluation of 3D blood flow patterns and wall shear stress in the normal and dilated thoracic aorta using flow-sensitive 4D CMR. J Cardiovasc Magn Reson. 2012; 14:14–84. [PubMed: 22300290]
33. Dolan JM, Meng H, Singh S, Paluch R, Kolega J. High fluid shear stress and spatial shear stress gradients affect endothelial proliferation, survival, and alignment. Ann Biomed Eng. 2011; 39:1620–1631. [PubMed: 21312062]
34. Torii R, Kalantzi M, Theodoropoulos S, Sarathchandra P, Xu XY, Yacoub MH. Predicting impending rupture of the ascending aorta with bicuspid aortic valve: spatiotemporal flow and wall shear stress: JACC Cardiovasc Imaging. 2013; 6:1017–1019. [PubMed: 24029373]
35. Spaziani G, Ballo P, Favilli S, et al. Clinical outcome, valve dysfunction, and progressive aortic dilation in a pediatric population with isolated bicuspid aortic valve. Pediatr Cardiol. 2014; 35:803–809. [PubMed: 24362596]
36. Ciotti GR, Vlahos AP, Silverman NH. Morphology and function of the bicuspid aortic valve with and without coarctation of the aorta in the young. Am J Cardiol. 2006; 98:1096–1102. [PubMed: 17027579]
37. Hoffman JL, Gray RG, Luann Minich L, et al. Screening for aortic aneurysm after treatment of coarctation. Pediatr Cardiol. 2014; 35:47–52. [PubMed: 23794012]
38. Cramer JW, Ginde S, Bartz PJ, Tweddell JS, Litwin SB, Earing MG. Aortic aneurysms remain a significant source of morbidity and mortality after use of Dacron((R)) patch aortoplasty to repair coarctation of the aorta: results from a single center. Pediatr Cardiol. 2013; 34:296–301. [PubMed: 22843204]
39. Madan N, Yau JL, Srivastava S, Nielsen JC. Comparison between proximal thoracic vascular measurements obtained by contrast-enhanced magnetic resonance angiography and by transthoracic echocardiography in infants and children with congenital heart disease. Pediatr Cardiol. 2013; 34:492–497. [PubMed: 22923009]
40. Lanzarini L, Larizza D, Prete G, et al. Aortic dimensions in Turner's syndrome: two-dimensional echocardiography versus magnetic resonance imaging. J Cardiovasc Med (Hagerstown). 2007; 8:428–437. [PubMed: 17502759]
41. Rivenes SM, Lewin MB, Stayer SA, et al. Cardiovascular effects of sevoflurane, isoflurane, halothane, and fentanyl-midazolam in children with congenital heart disease: an echocardiographic study of myocardial contractility and hemodynamics. Anesthesiology. 2001; 94:223–229. [PubMed: 11176085]
42. Harloff A, Zech T, Wegent F, Strecker C, Weiller C, Markl M. Comparison of blood flow velocity quantification by 4D flow MR imaging with ultrasound at the carotid bifurcation. AJNR Am J Neuroradiol. 2013; 34:1407–1413. [PubMed: 23413247]

43. Petersson S, Dyverfeldt P, Ebbers T. Assessment of the accuracy of MRI wall shear stress estimation using numerical simulations. J Magn Reson Imaging. 2012; 36:128–138. [PubMed: 22336966]

44. Pasta S, Rinaudo A, Luca A, et al. Difference in hemodynamic and wall stress of ascending thoracic aortic aneurysms with bicuspid and tricuspid aortic valve. J Biomech. 2013; 46:1729–1738. [PubMed: 23664314]

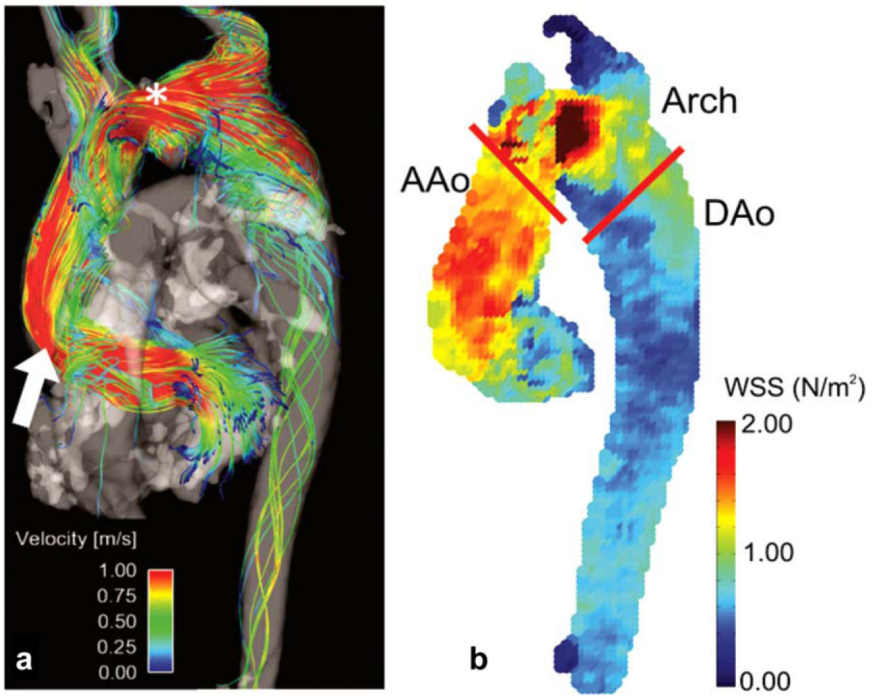

FIGURE 1.

The 4D flow findings in a pediatric BAV patient with a gothic-shaped arch and history of aortic coarctation repair. **A**: Streamline visualization of systolic blood flow at peak systole. Note the high velocity outflow jet impinging on the lateral wall of the AAo (white arrow) and the high velocity flow within the arch of the aorta (*). **B**: Maximum intensity projection of absolute WSS_{sys}, with high WSS values corresponding with regions of high velocity flow and jet impingement in A. The red lines indicate the aortic region divisions used for regional analysis in the ascending aorta (AAo), arch and descending aorta (DAo).

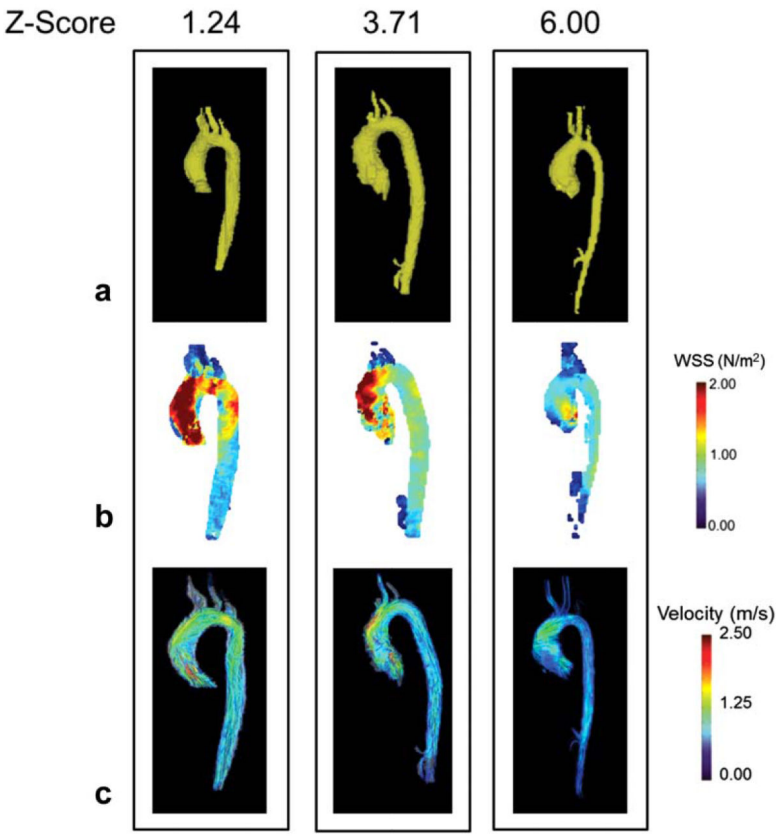

FIGURE 2.

The 3D segmentation (**A**), wall shear stress maximum intensity projection (**B**), and systolic 3D streamlines (**C**) in three patients with varying degrees of aortic dilatation as measured by aortic root Z-score. Patients with higher levels of WSS appear to have higher velocity outflow jets (denoted by red streamlines) in the ascending aorta. While it appears that WSS is inversely proportional to aortic root Z-score in these individual patients, cohort analysis did not support this relationship. [Color figure can be viewed in the online issue, which is available at wileyonlinelibrary.com.]

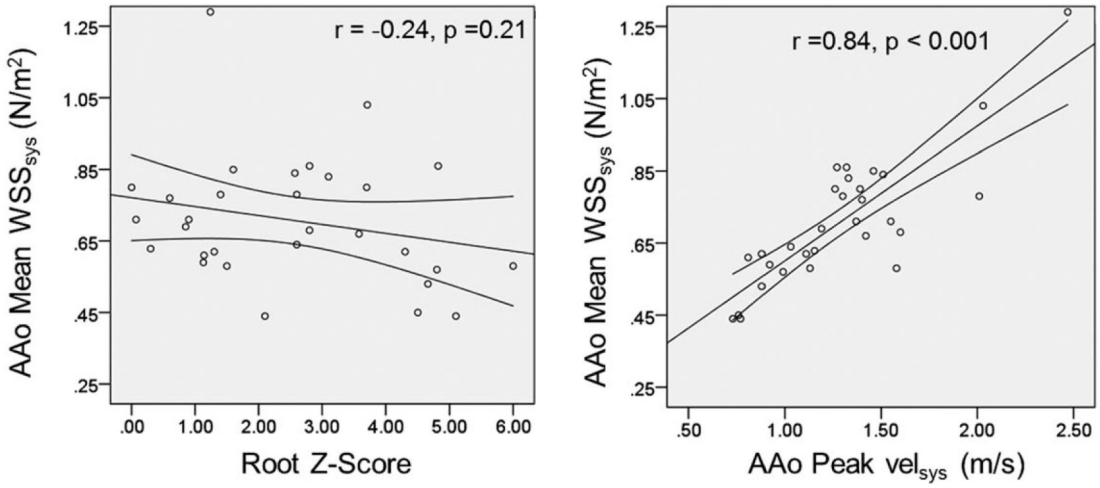

FIGURE 3.

Scatter plots demonstrating relationships between aorta (AAo) root Z-score (left) and ascending aorta (AAo) max systolic velocities (vel_{sys}) (right) with AAo systolic wall 3D shear stress (WSS_{sys}).

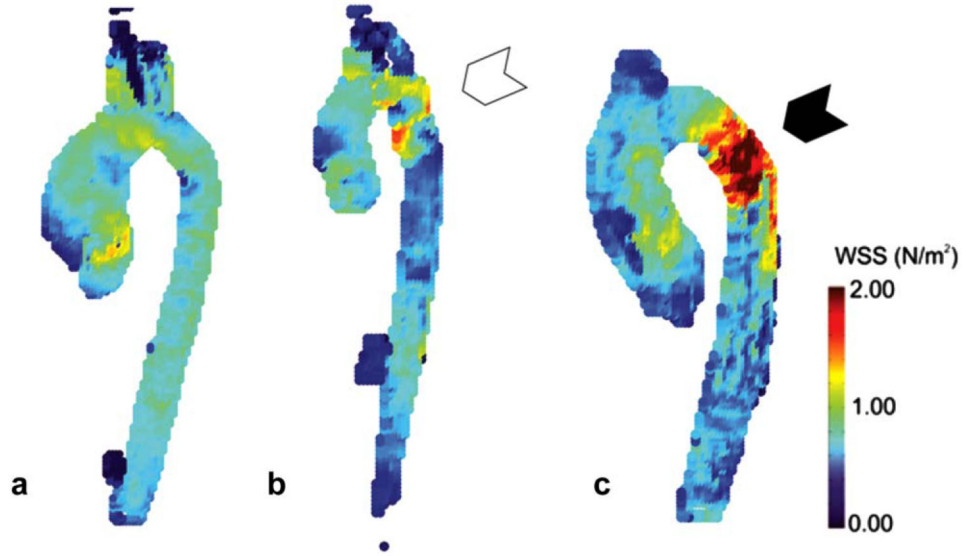

FIGURE 4.

Examples of absolute WSS_{sys}, maximum intensity projections in a patient with no aortic coarctation (**A**), nonrepaired aortic coarctation (**B**), and repaired aortic coarctation (**C**). In A, there is an asymmetric distribution of WSS in the ascending aorta characterized by higher WSS values on the lateral wall, but no evidence of localized elevations in the descending aorta. In B, the white arrow points to the coarctation location where there is a band of increased WSS near the narrowing and into the proximal descending aorta. Finally in C, the black arrow points to the location of coarctation repair where there is a large region of increased WSS that extends backward into the aortic arch as well as projecting onto the lateral wall of the descending aorta. [Color figure can be viewed in the online issue, which is available at wileyonlinelibrary.com.]

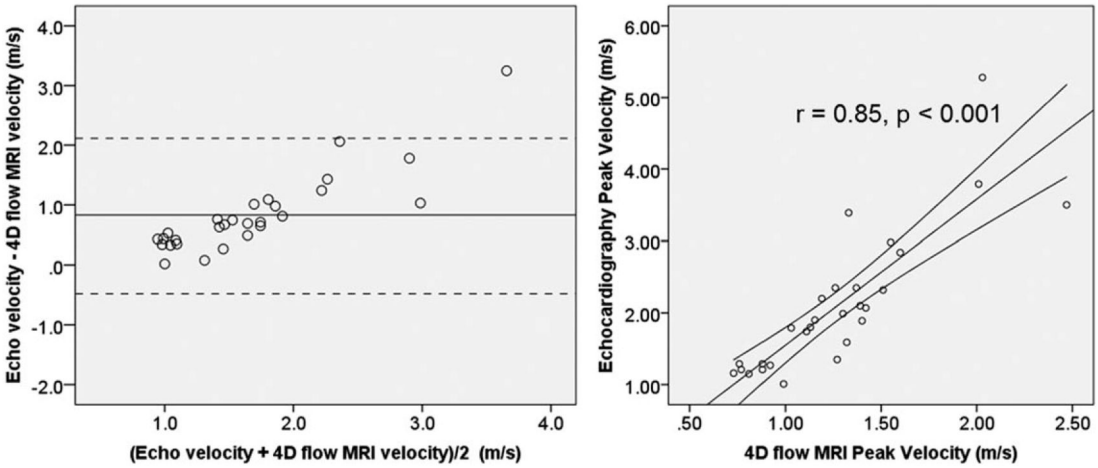

FIGURE 5.

Bland-Altman plot (left) and correlation scatter plot (right) comparing echocardiographic assessment of peak aortic valve velocity with peak velocity measured using 4D flow MRI. The mean difference on the Bland-Altman plot is indicated by the horizontal solid line and is equal to 0.83 m/s demonstrating a systematic underestimation of peak velocity by 4D flow MRI relative to echocardiography. The 95% confidence intervals for the difference in velocity measurements are indicated by the horizontal dashed lines.

TABLE 1

Patient Characteristics

	Mean±SD	Range
Age (years)	13.9±4.4	[3.4,20.7]
BSA (m^2)	1.5±0.4	[0.6,2.2]
Aortic stenosis severity	1.0±1.3	[0,4]
Aortic insufficiency severity	0.6±0.9	[0,3]
Aortic root Z-score	2.5±1.7	[0,6]
Ascending aorta Z-score	2.4±2.3	[−2.3,6.4]
Indexed aortic root diameter (mm/m^2)	21.2±5.8	[14.1,42.4]
Indexed ascending aorta diameter (mm/m^2)	20.4±6.1	[13.6,41.5]
BAV morphology (number)		
Right-left	25	
Right-non	5	

TABLE 2

Regional Hemodynamic Findings

		Mean±SD
Max WSS_{sys} (N/m^2)	AAo	1.3±0.4
	Arch	1.2±0.3
	DAo	1.2±0.3
Mean WSS_{sys} (N/m^2)	AAo	0.7±0.2
	Arch	0.7±0.2
	DAo	0.8±0.2
Peak Vel_{sys} (m/s)	AAo	1.29±0.4
	Arch	1.06±0.3
	DAo	1.00±0.2

TABLE 3

Subgroup Analysis of Hemodynamics in the Thoracic Aorta of Bicuspid Aortic Valve Disease Patients with Aortic Coarctation or Coarctation Repair

		No coarctation (n=20)	Non- repaired coarctation (n=3)	Coarctation repair (n=7)	*P*-value[a]
Age (years)		13.7±3.6	7.8±5.2	16.9±4.2	0.007
BSA (m^2)		1.5±0.4	1.0±0.5	1.7±0.3	0.09
Aortic stenosis severity		1.2±1.3	0.7±1.2	0.9±1.5	0.78
Aortic insufficiency severity		0.8±1	0.3±0.6	0.4±0.8	0.61
Aortic root Z-score		2.7±1.8	2.2±2	2.2±1.7	0.77
Ascending aorta Z-score		2.9±2.3	2±2.3	0.8±2	0.10
Indexed aortic root diameter (mm/m^2)		21±6	25.3±7.1	19±3	0.29
Indexed ascending aorta Diameter (mm/m^2)		21.3±6	24.1±8.6	15.9±2.6	0.06
Max WSS_{sys} (N/m^2)	AAo	1.3±0.4	1.0±0.3	1.5±0.6	0.29
	Arch	1.1±0.2	1.2±0.1	1.6±0.4	0.001
	DAo	1.1±0.2	1.2±0.4	1.4±0.3	0.011
Mean WSS_{sys} (N/m^2)	AAo	0.7±0.2	0.6±0.1	0.8±0.2	0.32
	Arch	0.7±0.1	0.6±0.1	0.8±0.3	0.15
	DAo	0.8±0.3	0.5±0.1	0.8±0.1	<0.001
Peak Vel_{sys} (m/s)	AAo	1.3±0.4	1.0±0.3	1.4±0.5	0.32
	Arch	1.0±0.2	0.8±0.1	1.4±0.3	<0.001
	DAo	1.0±0.2	0.7±0.2	1.2±0.3	0.016

[a] *P*-value from ANOVA.